*Electronic Supplementary Information for*

# Herringbone to Cofacial Solid State Packing via H-bonding in Diketopyrrolopyrrole (DPP) based Molecular Crystals: Influence on Charge Transport

Joydeep Dhar, Durga Prasad Karothu, and Satish Patil*

Solid State and Structural Chemistry Unit, Indian Institute of Science, Bangalore 560012

E-mail: satish@sscu.iisc.ernet.in

## Table of contents                                            page no

## Measurements and general methods:

All the chemicals were received from commercial sources and used without further purification. The $^1$H and $^{13}$C NMR spectra of two DPP derivatives were recorded on Bruker Avance NMR spectrometer using CDCl$_3$ and TMS as solvent and internal standard, respectively. ESI mass spectra were recorded on Thermo LCQ Deca XP MAX spectrometer with a resolution of 1.0 Da. The optical absorption spectra were collected in chloroform on Perkin-Elmer (Lambda 35) spectrometer at room temperature. Steady state fluorescence spectra of PDPP-MH and TDPP-MH were monitored in Horiba Jobin Yvon Fluorolog3 fluorometer and fluorescence quantum yield was determined using integrated sphere attached as an additional accessory to the fluorometer. Time resolved fluorescence decay measurements were carried out in chloroform in Horiba Jobin Yvon Fluorocube 01-NL lifetime spectrometer using time correlated single photon counting (TCSPC) method with a pico-second laser (469 nm, 25ps). Transmission electron microscopy (TEM) images were taken in FEI Tecnai T20 and Zeol field emission transmission electron microscope at 160 kV and 200 kV, respectively at room temperature after drop-casting the sample on copper grid dissolved in $o$-dichlorobenzene (ODCB)/acetonitrile (ACN) (8:1). Single crystal X-ray diffraction data was collected on an Oxford Xcalibur (Mova) diffractometer equipped with an EOS CCD detector with Mo Kα radiation (λ = 0.71073 Å). Temperature was maintained at 110 K while collecting the data using the cryojet-HT controller. Differential Scanning Calorimetry (DSC) analysis was performed in Mettler Toledo DSC1 system with N$_2$ flow of 40 mL/min at a heating and cooling rate of 5 °C/min with an empty Al pan taken as standard. Hot-stage polarising microscopy images were taken in Olympus BX-51 microscope with a programmable temperature controller. Redox properties of the two molecules were evaluated by cyclic voltammetry experiment (CH instrument). Ag/AgCl was used as reference electrode. Platinum (Pt) disk and wire were employed for working and counter electrodes. Dry chloroform and 0.1 (M) tetrabutylammonium hexafluorophosphate were used as solvent and supporting electrolyte, respectively. Ferrocene/ferrocenium (Fc/Fc$^+$) couple was used as standard electrochemical reference. The energies of HOMO and LUMO and corresponding band gap were calculated from the respective oxidation and reduction potential. Since ferrocene oxidizes to ferrocenium ion at 0.3 V with respect to Ag/AgCl system the position of HOMO and LUMO were computed from the equation **1** and the electrochemical band gap was determined from the difference between them.

$$HOMO = -(E_{ox} + 4.5)\ eV;\quad LUMO = -(E_{red} + 4.5)\ eV \tag{1}$$

The single crystal OFET devices were fabricated in bottom-gate-bottom-contact (BGBC) configuration. First, 190 nm thick $SiO_2$ dielectric layer was deposited on a highly n-type doped Si substrate by dry oxidation method. The capacitance was measured to be 18.2 $nF/cm^2$. Hexamethyldisilazane (HMDS) were vacuum deposited on top of $SiO_2$ layer. Then, 100 nm thick gold (Au) source and drain electrodes were patterned photolithographically with variable channel length. The samples dissolved in ODCB/ACN (8:1) drop-casted on channel region and allowed solvent to evaporate slowly and crystals to grow. Then the devices were kept at 80 °C for 2 h in vacuum. The current-voltage measurements were carried out in open atmosphere at room temperature using DC Probe-station. Mobility of the charge carriers were computed from the saturation region of the plot following the formula

$$\left(I_{SD}\right)_{sat} = \left(\frac{W}{2L}\right) C\mu \left(V_G - V_T\right)^2$$

where, $(I_{SD})_{sat}$, L, W, C, $\mu$, $V_G$ and $V_T$ represent source-drain current in saturation region, channel length, channel width, capacitance of the dielectric layer, charge-carrier mobility, gate voltage and threshold voltage, respectively.

**Computational Methods:**

The B3LYP function with 6-31g* basis set was employed for the geometry optimization in Gaussian 09 suite programme. Charge transfer integrals were estimated applying Koopmans's theorem and the 'energy splitting in dimer' KT-ESD method. According to this approach, the charge transfer integral '*t*' for hole transport equals half the energy difference between HOMO and HOMO-1 and for electron transport between LUMO and LUMO+1.[1] Dimer structures were obtained from the experimental crystal structures by extracting the two closest-lying molecules in each of the three crystallographic directions. Single point energies of dimers were calculated with density functional theory employing the wB97xd [2] functional and the 6-31G* basis set. Test calculation with other functionals (LSDA, BLYP, B3LYP, and with Hartree-Fock theory) show that the energy level splitting is almost independent of the method.

**Synthesis of Mono-Hexyl DPP Derivatives.**

**2-hexyl-3,6-diphenylpyrrolo[3,4-c]pyrrole-1,4(2H,5H)-dione    (PDPP-MH):**    3,6-diphenyl pyrrolo[3,4-c]pyrrole-1,4(*2H,5H*)-dione (PDPP) was synthesized following the reported procedure in the literature.[3] The mono-alkylation reaction was carried out in a controlled manner. PDPP (0.2 g, 0.69 mmol) was dissolved in 40:20 mL of NMP/DMF mixture and stirred for 30 min in an inert atmosphere. Then *t*-BuOK (0.8 g, 0.72 mmol) was added to it and heated at 90 °C for 1 h. Next, drop-wise 1-bromohexane (0.12 g, 0.75 mmol) dissolved in DMF was added in three portions with a gap of 1 h for each addition. After completion of addition, the reaction was allowed to continue for next 5 h at 125°C with intermittent TLC checking. Water was added to quench the reaction. Solvents were distilled out. The compound was eluted by hexane/ethyl acetate in column chromatography (Yield: 23 %). $^1$H NMR (400 MHz, CDCl$_3$, ppm): δ 8.82 (s, 1H), 8.29-8.27 (m, 2H), 8.83-8.81 (m, 2H), 7.59-7.51 (m, 6H), 3.85-3.81 (t, 2H), 1.67-1.61 (m, 2H), 1.3-1.2 (m, 6H), 0.85-0.82 (t, 3H). $^{13}$C NMR (100 MHz, CDCl$_3$, ppm): δ 163.48, 162.68, 148.23, 145.02, 132.01, 131.27, 129.14, 128.86, 128.21, 128.01, 127.75, 110.99, 109.74, 42.21, 31.23, 29.44, 26.54, 22.48, 13.94. Elemental Analysis: Calc. (%): (C$_{24}$H$_{24}$N$_2$O$_2$): C, 77.39; H, 6.49; N, 7.52 Found (%): C, 77.88; H, 6.15; N, 7.71. (ESI-MS) calculated for C$_{24}$H$_{24}$N$_2$O$_2$ (M)$^+$: m/z: 371.4

**2-hexyl-3,6-di(thiophen-2-yl)pyrrolo[3,4-c]pyrrole-1,4(2H,5H)-dione   (TDPP-MH):** TDPP-MH was synthesized by alkylating 3,6-di(thiophen-2-yl)-pyrrolo[3,4-c]pyrrole-1,4(*2H,5H*)-dione (TDPP) in a similar manner.[4] TDPP (0.5 gm, 1.66 mmol) and potassium carbonate (0.23 gm, 1.66 mmol) were taken in DMF (60 mL), heated at 90 °C for 1h. Then slowly 1-bromohexane (0.27 gm, 1.67 mmol) was added to the reaction mixture in three portions and temperature was raised to 125 °C and continued for next 5 h. Later DMF was distilled out, washed with water and extracted in CHCl$_3$. The crude product was purified by column chromatography (Yield: 25%). $^1$H NMR (400 MHz, CDCl$_3$, ppm): δ 8.9-8.88 (dd, 1H) 8.46 (s, 1H), 8.37-8.36 (dd, 1H), 7.69-7.67 (dd, 1H), 7.63-7.62 (dd, 1H), 7.33-7.32 (dd, 1H), 7.27-7.25 (dd, 1H), 4.12-4.08 (t, 2H), 1.82-1.74 (m, 2H), 1.49-1.37 (m, 6H), 0.92-0.89 (t, 3H). $^{13}$C NMR (100 MHz, CDCl$_3$, ppm): δ 162.15, 161.35, 140.55, 136.28, 136.26, 135.55, 132.01, 130.78, 129.80, 129.10, 128.64, 108.61, 108.13, 42.26, 31.42, 29.93, 26.55, 22.56, 14.01. Elemental Analysis: Calc. (%):

($C_{20}H_{20}N_2O_2S_2$): C, 62.47; H, 5.24; N, 7.29 Found (%): C, 63.21; H, 5.65; N, 7.55. (ESI-MS) calculated for $C_{20}H_{20}N_2O_2S_2$ (M)$^+$: m/z: 383.4
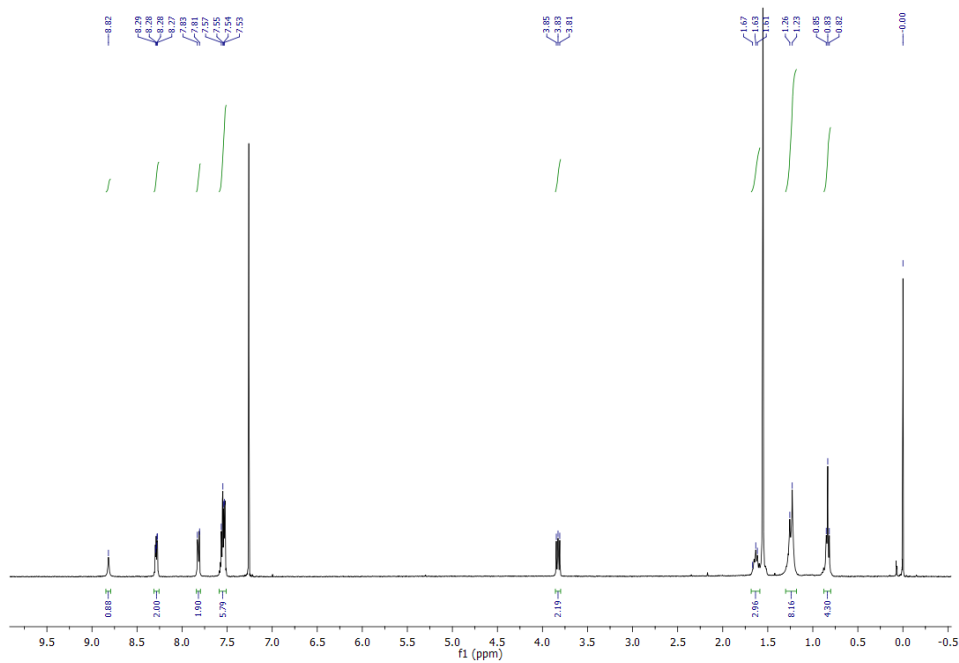


**S 1.** $^1$H NMR spectrum of PDPP-MH
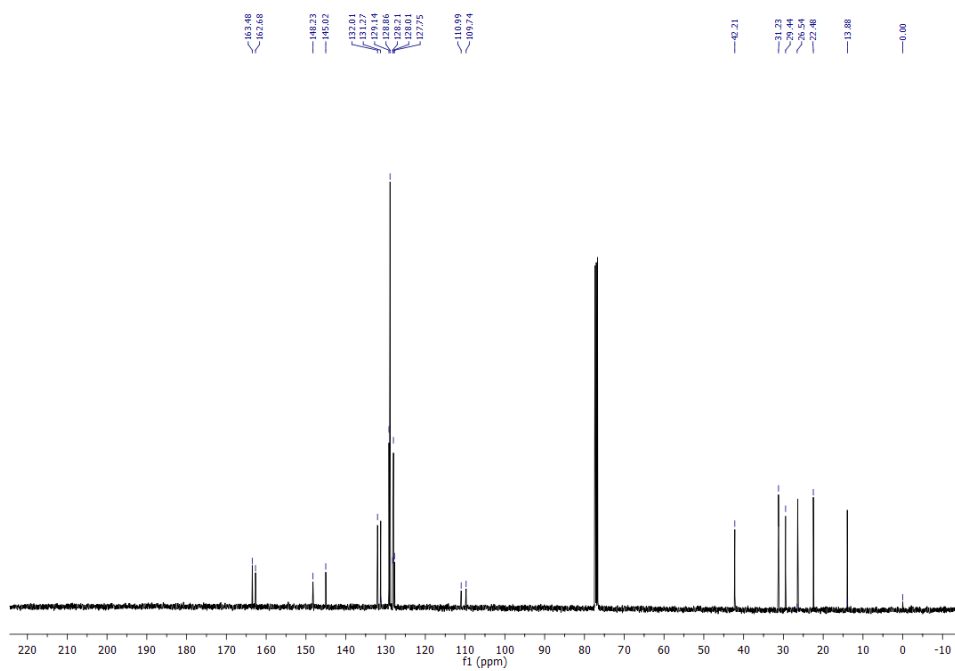


**S 2.** $^{13}$C NMR spectrum of PDPP-MH
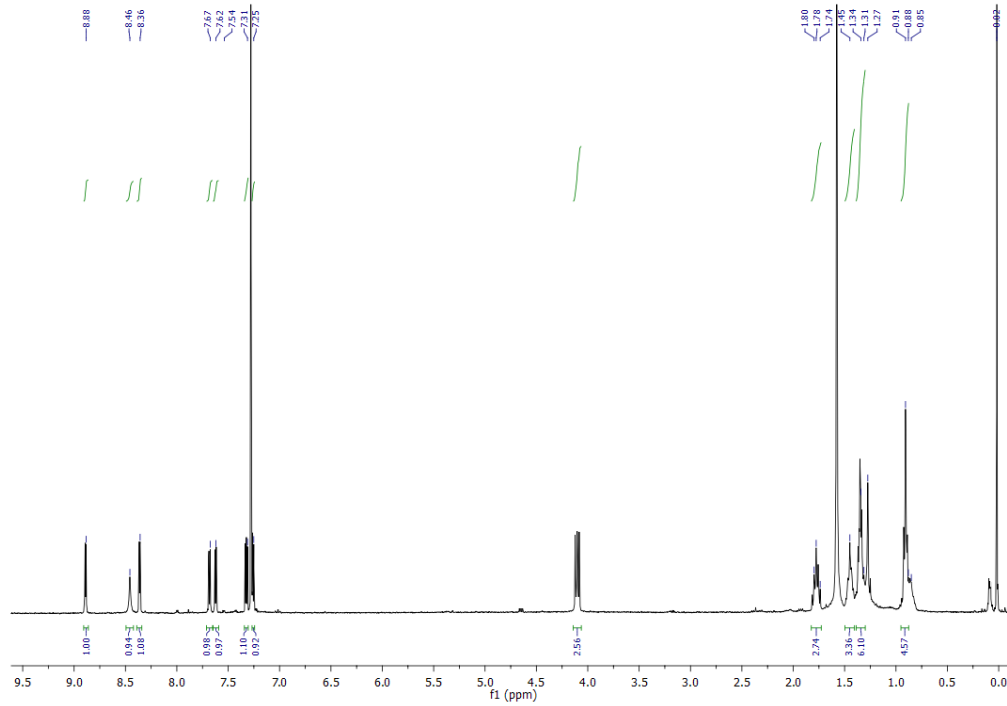
**S 3.** $^1$H NMR spectrum of TDPP-MH
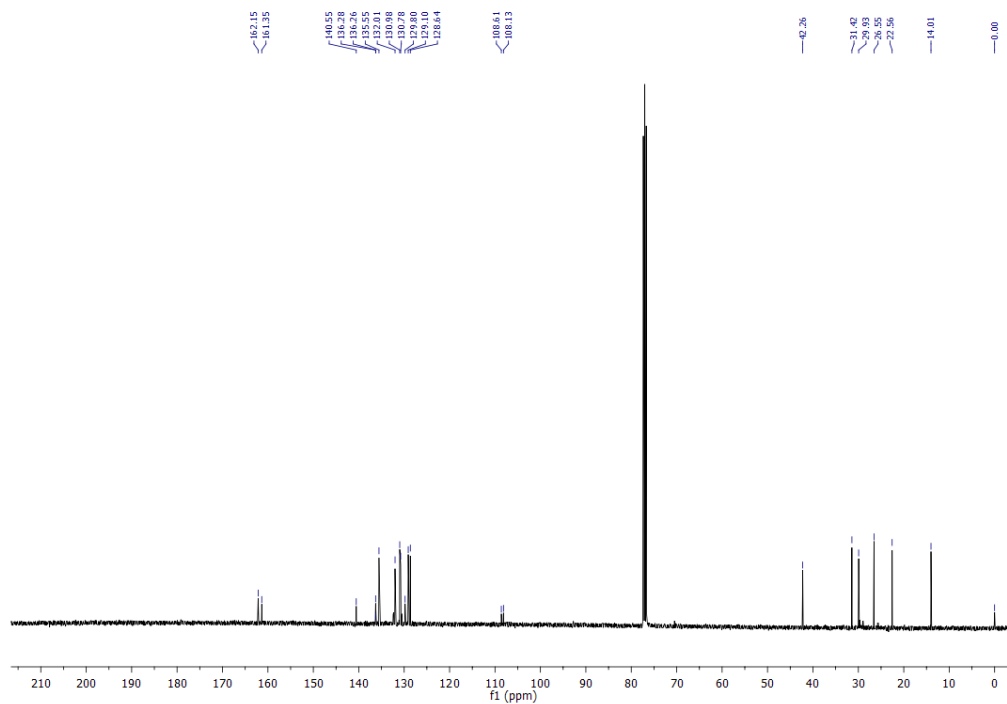


**S 4.** $^{13}$C NMR spectrum of TDPP-MH
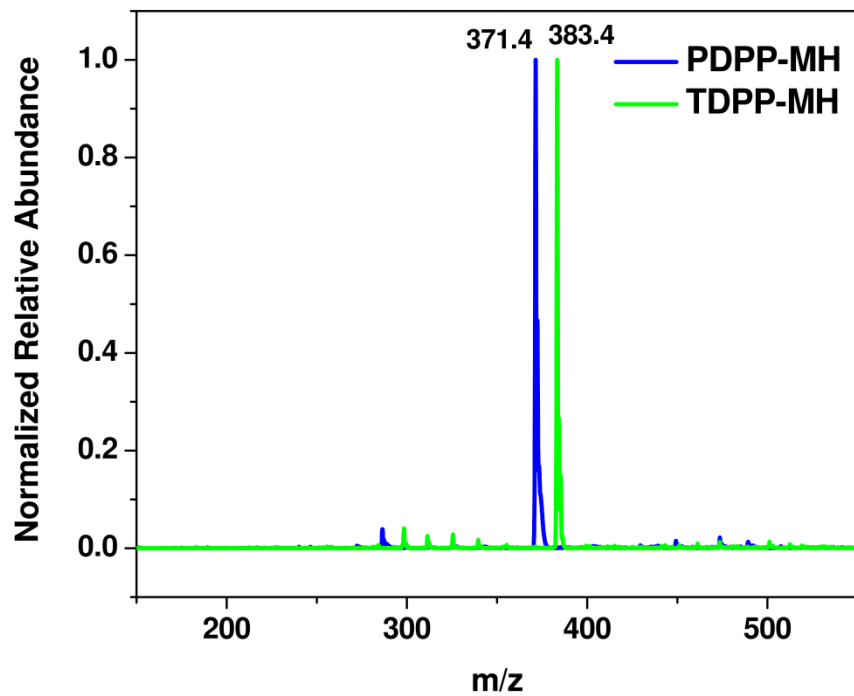
**S 5.** ESI Mass spectra of two DPP derivatives.
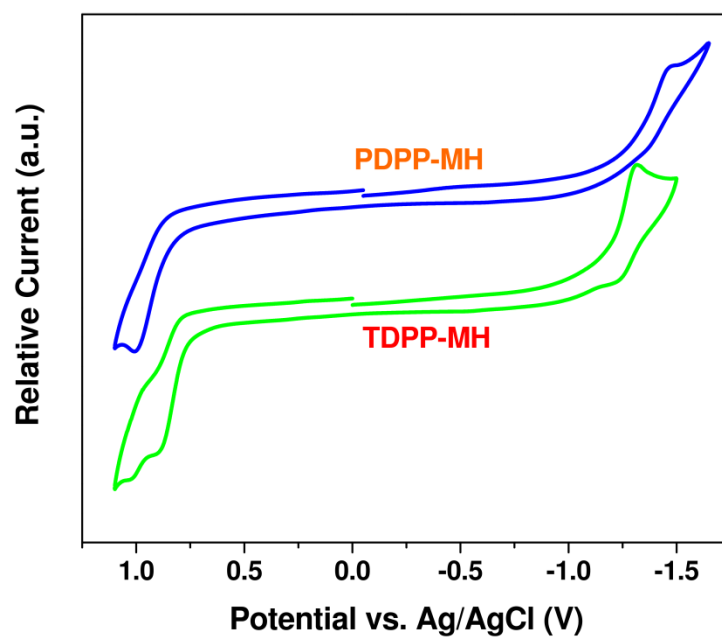


**S 6.** Cyclic voltammograms of DPP derivatives recorded in dry chloroform.
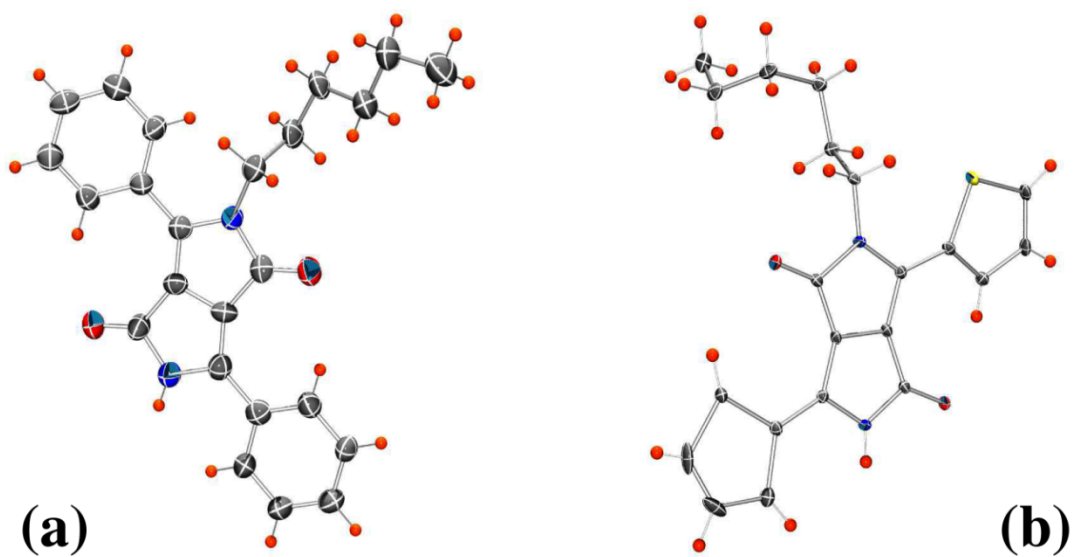
**S 7**. ORTEP representation of PDPP-MH (a) and TDPP-MH (TDPP-MH is drawn at 50% probability level).
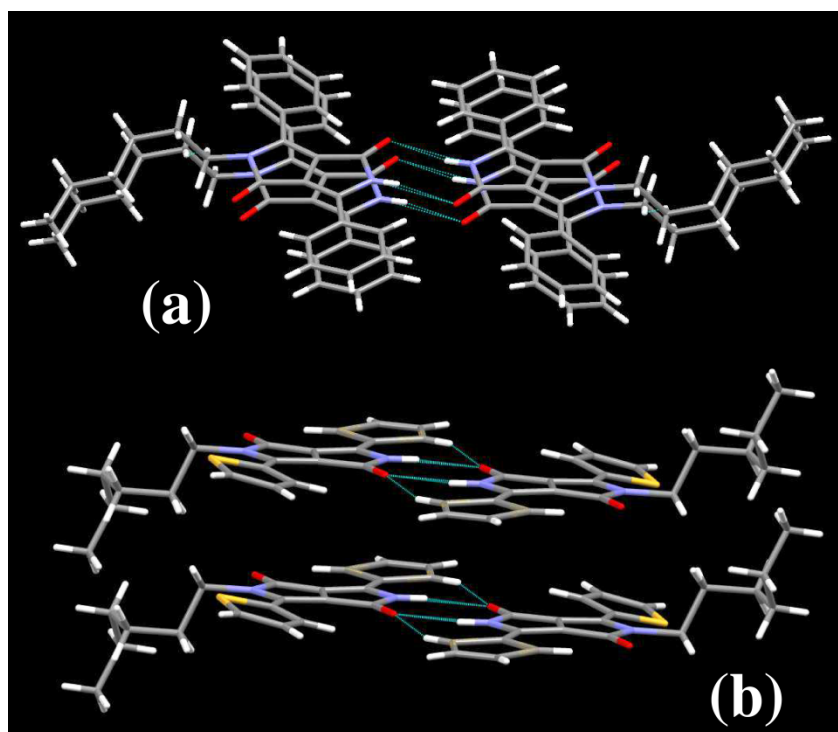


**S 8**. H-bond mediated cofacial packing in PDPP-MH (a) and TDPP-MH (b) single crystal.
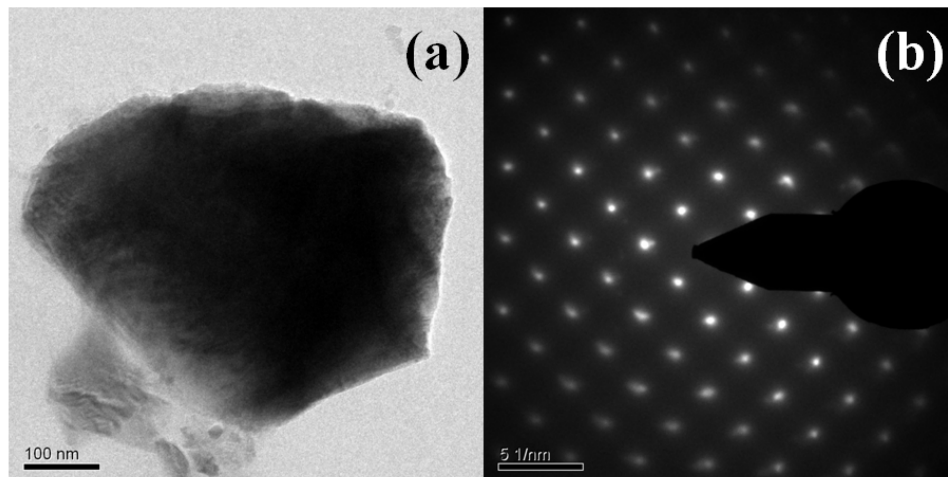
**S 9.** Bright field (a) and selected area electron diffraction (SAED) pattern from single crystalline TDPP-DH crystallite.
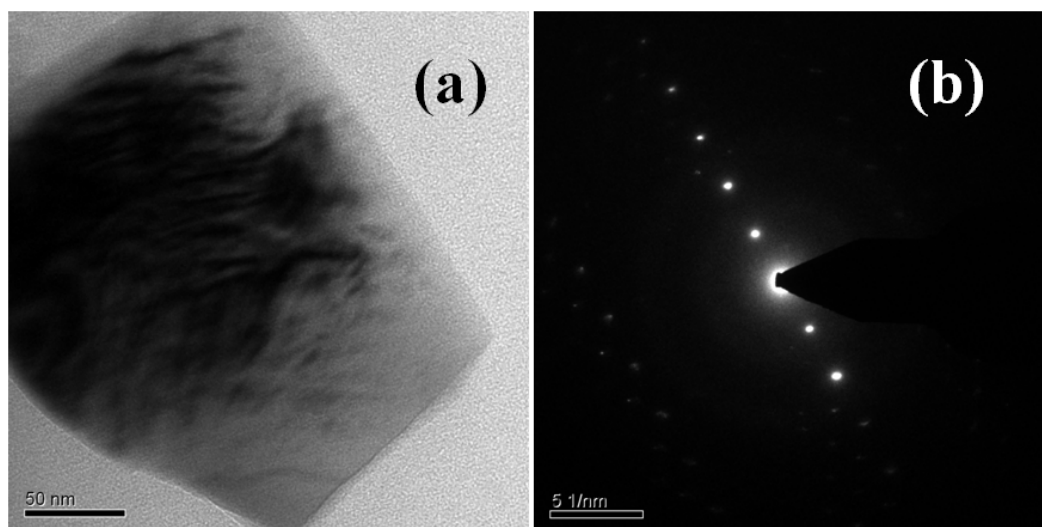


**S 10.** Bright field (a) and selected area electron diffraction (SAED) pattern from single crystalline TDPP-DH crystallite.
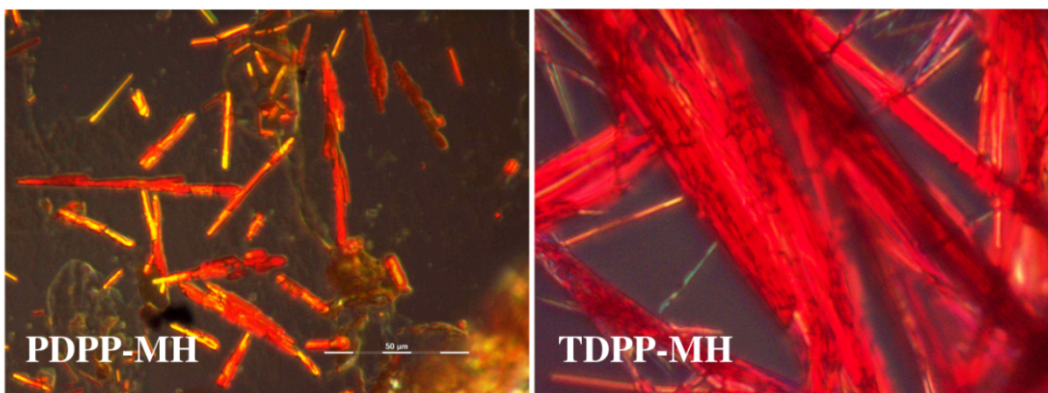
**S 11.** Polarising microscope images of PDPP-MH and TDPP-MH at 200 °C drop-casted on glass-slides.
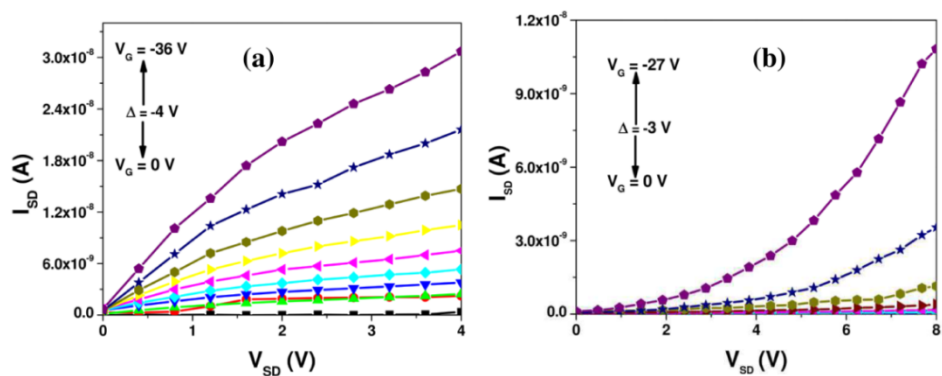


**S 12.** Output characteristics of PDPP-DH (a) and TDPP-DH (b) OFET devices.
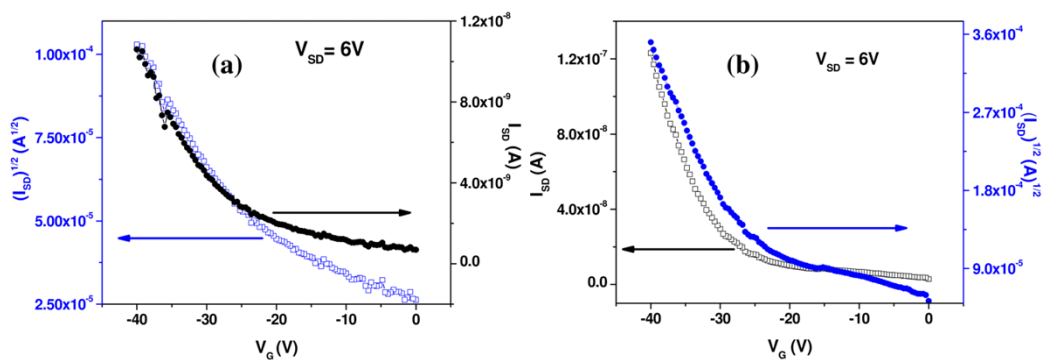


**S 13.** Transfer characteristics of PDPP-MH (a) and TDPP-MH (b) OFET devices.
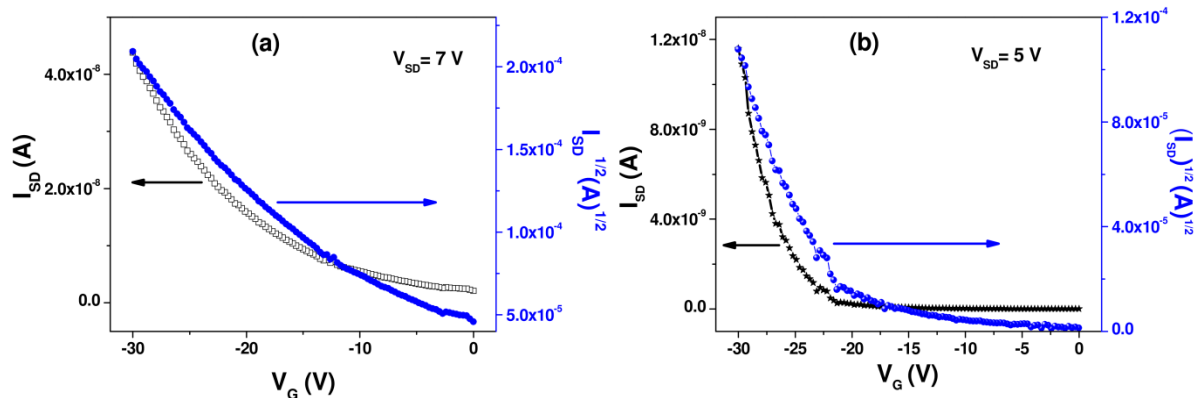
**S 14.** Transfer characteristics of PDPP-DH (a) and TDPP-DH (b) OFET devices.
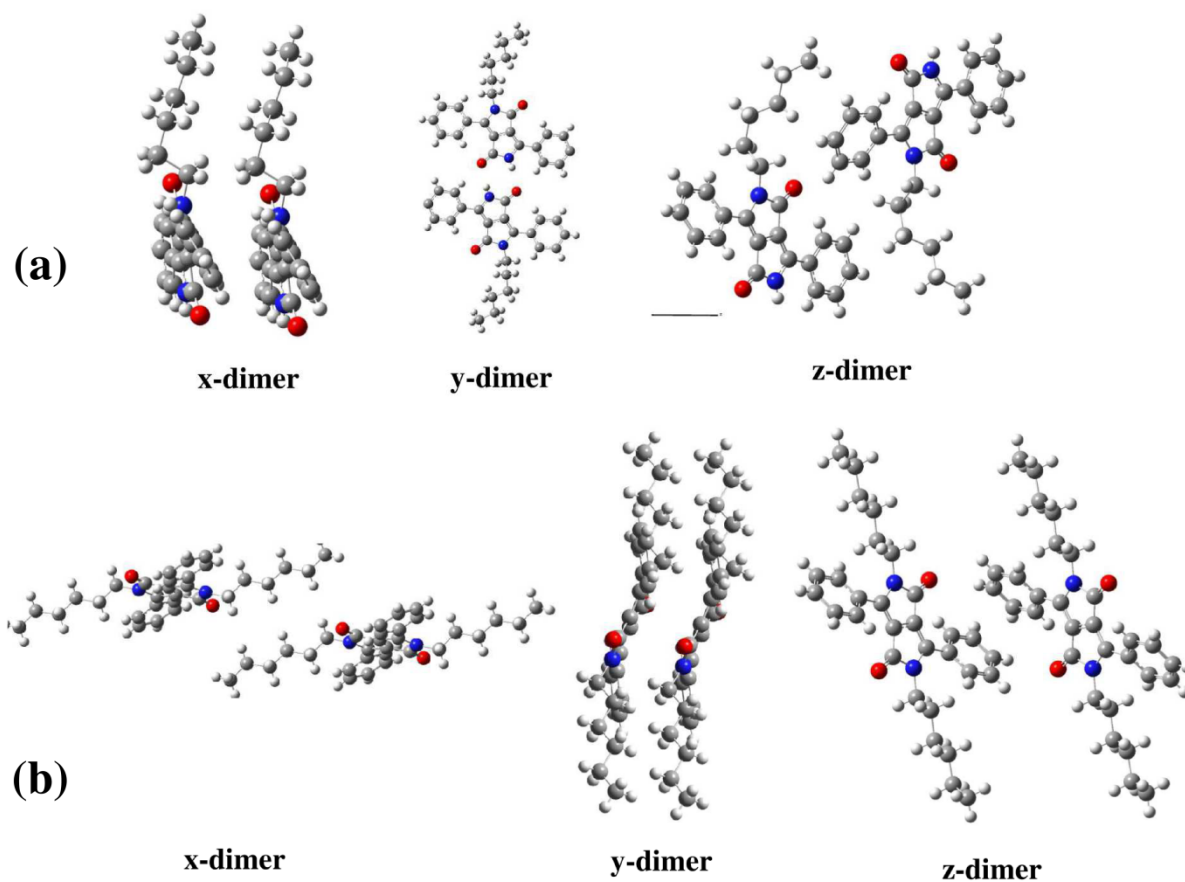


**S 15.** Dimer structures of the two closest-lying molecules of PDPP-MH (a) and PDPP-DH (b) in each of the three crystallographic directions.
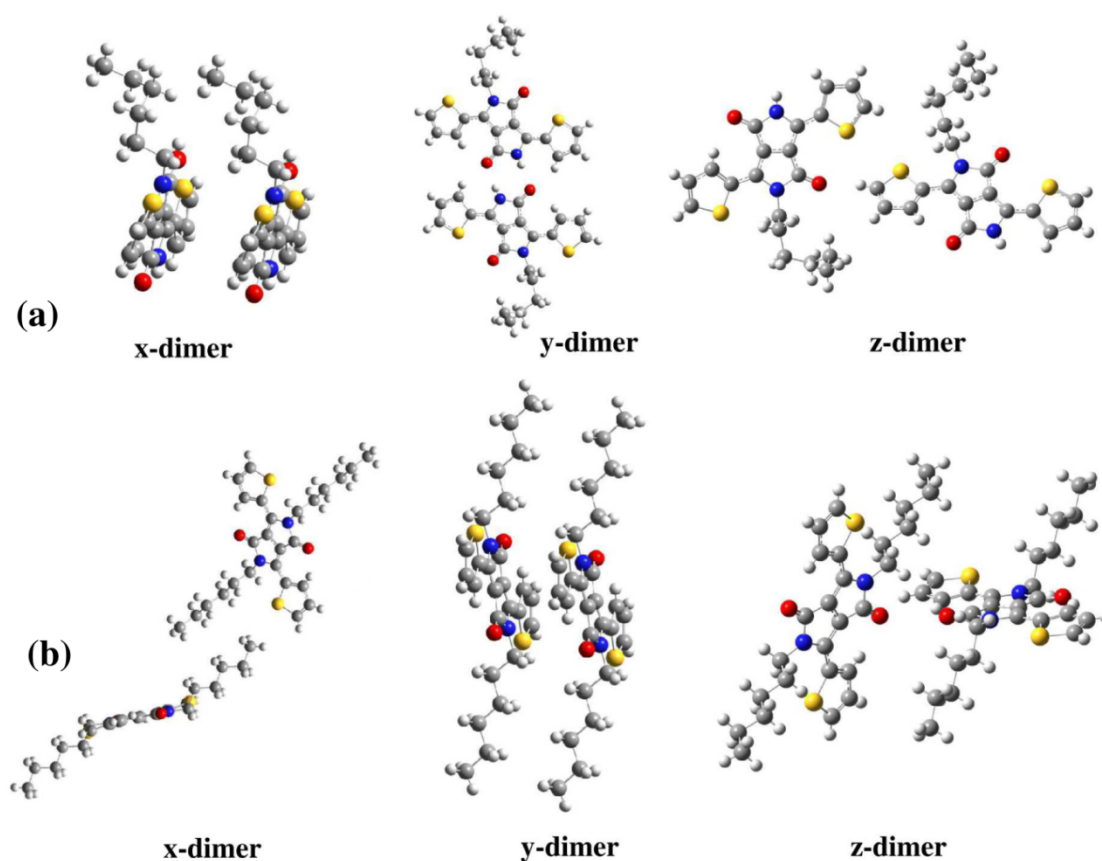
**S 16.** Dimer structures of the two closest-lying molecules of TDPP-MH (a) and TDPP-DH (b) in each of the three crystallographic directions.

**Table S1.** Summary of the photophysical, electrochemical and theoretical properties of the two mono-hexyl DPP derivatives

| Compounds | Optical Properties | | | | Electrochemical properties[a] | | | DFT[b] |
|---|---|---|---|---|---|---|---|---|
| | $\lambda_{abs}$ (max) (nm) | $\varepsilon_{max}$ ($M^{-1}cm^{-1}$) | $\lambda_{em}$ (max) (nm) | Stokes Shift (eV) | HOMO (eV) | LUMO (eV) | $E_g^{elec}$ (eV) | $E_g$ (eV) |
| PDPP-MH | 465, 490 | 15000 | 520, 550 | 0.19 | -5.51 | -3.03 | 2.48 | 2.78 |
| TDPP-MH | 500, 540 | 20300 | 550, 595 | 0.05 | -5.4 | -3.2 | 2.20 | 2.48 |

[a]The data obtained from cyclic voltammetry with reference to the Ag/AgCl electrode and ferrocene/ferrocenium (Fc/Fc+) couple as standard. [b]The values obtained from the difference between the HOMO and LUMO energy levels optimized at the B3LYP/6-31g* basis set.

**Table S2.** The summary of transfer integral ($t$) values in three crystallographic directions

| Compounds | $t^+$ (x) | $t^-$ (x) | $t^+$ (y) | $t^-$ (y) | $t^+$ (z) | $t^-$ (z) |
| --- | --- | --- | --- | --- | --- | --- |
| | | | (eV) | | | |
| PDPP-MH | 0.05 | 0.075 | 0.005 | 0.005 | 0.065 | 0.065 |
| PDPP-DH | - | - | 0.015 | 0.015 | 0.095 | 0.1 |
| TDPP-MH | 0.015 | 0.02 | 0.025 | 0.02 | 0.125 | 0.125 |
| TDPP-DH | 0.015 | 0.01 | 0.075 | 0.14 | 0.015 | 0.01 |

$t^+$ and $t^-$ are the transfer integrals associated with the hole and electron transport, respectively.

x, y, and z indicate the crystallographic direction

**References.**

1. V. Coropceanu, J. Cornil, D. A. da Silva Filho, Y. Olivier, R. Silbey and J.-L. Bredas, *Chem. Rev.*, 2007, 107, 926-952.
2. J.-D. Chai and M. Head-Gordon, *Phys. Chem. Chem. Phys.*, 2008, 10, 6615-6620.
3. A. R. Rabindranath, Y. Zhu, I. Heim and B. Tieke, *Macromolecules*, 2006, 39, 8250-8256.
4. A. B. Tamayo, B. Walker and T. Q. Nguyen, *J. Phys. Chem. C*, 2008, 112, 11545-11551.